NEUROSCIENCE

Chemogenetic activation of microglial Gi signaling decreases microglial surveillance and impairs neuronal synchronization

Shunyi Zhao[1,2,3], Lingxiao Wang[1,2], Dimitrios Kleidonas[1,3], Fangfang Qi[1,3], Yue Liang[1,3], Jiaying Zheng[1,3], Anthony D. Umpierre[1], Long-Jun Wu[1,3]*

Microglia actively survey the brain and dynamically interact with neurons to maintain brain homeostasis. Microglial Gi protein–coupled receptors (Gi-GPCRs) play a critical role in microglia-neuron communications. However, the impact of temporally activating microglial Gi signaling on microglial dynamics and neuronal activity in the homeostatic brain remains largely unknown. In this study, we used Gi-based designer receptors exclusively activated by designer drugs (Gi-DREADD) to selectively and temporally modulate microglial Gi signaling pathway. By integrating this chemogenetic approach with in vivo two-photon imaging, we observed that exogenous activation of microglial Gi signaling transiently inhibited microglial process dynamics, reduced neuronal activity, and impaired neuronal synchronization. These altered neuronal functions were associated with a decrease in interactions between microglia and neuron somata. Together, this study demonstrates that acute, exogenous activation of microglial Gi signaling regulates neuronal circuit function, offering a potential pharmacological target for the neuromodulation through microglia.

INTRODUCTION

Microglia actively survey the brain through their dynamic processes (*1*–*3*). Their surveillance and interactions with neurons have been linked to neuronal activity changes (*4*, *5*). Specifically, physical microglia-neuron interactions have been associated with dampening hyperactive neurons, promoting hypoactive neuronal activity, or maintaining the hypoactive state of neurons (*6*–*9*). These functions are partially mediated by microglial Gi protein–coupled receptors (Gi-GPCRs), such as the P2Y12 receptor (*6*, *8*, *9*). Genetic knockout of the P2Y12 receptor in microglia has been shown to elevate anxiety, disrupt general anesthesia, and increase seizure severity in mice (*6*, *8*–*12*). In addition, microglial-specific Gi signaling inhibition through pertussis toxin expression (PTX) decreased microglial surveillance and increased neuronal activity (*13*). These findings indicate that microglial Gi-GPCRs are crucial in regulating neuronal activity and emerge as intriguing targets for neuromodulation. However, the impact of specifically activating microglial Gi signaling on the neural circuit function remains unknown.

To selectively activate microglial Gi signaling, recent studies used a chemogenetic tool, designer receptors exclusively activated by designer drugs (DREADD) (*14*). Using these engineered Gi-GPCRs, we demonstrated that microglial Gi-DREADD activation could mimic endogenous Gi-mediated chemotaxis (*15*). Furthermore, this method has been successfully applied in disease conditions, such as pain and epilepsy, to explore function of microglial Gi signaling (*16*). Acute activation of microglial Gi signaling after seizure onset increased microglia-neuron soma interactions, altered microglial morphology, and decreased seizure severity (*17*). Chronic activation of microglial Gi signaling after peripheral nerve injury decreased the inflammatory cytokine release and ameliorated chronic pain (*18*, *19*). These results indicate the potential of microglial Gi signaling to relieve pathological neuron hyperactivity.

In the current study, we used two-photon imaging and microglial chemogenetics to investigate how microglial Gi signaling influences microglia-neuron interaction and neural circuit function in the homeostatic brain. We observed that microglia retracted their processes after Gi-DREADD activation. This morphology alteration led to decreased interactions with neuronal soma, which was associated with reduced neuronal activity and impaired synchronization. Our findings address an intriguing question of how microglia are integrated into neuronal circuits. Regulation of neural circuit function through microglial Gi signaling could provide an important pharmacological target for the neuromodulation.

RESULTS

Chemogenetic activation of microglial Gi signaling decreases microglial process surveillance

Genetically inhibiting microglial Gi signaling by PTX decreases microglial surveillance (*13*). To activate Gi signaling in microglia, we induced hM4Di (Gi-DREADD) expression in microglia using a $Tmem119^{CreER/+}$:$R26^{hM4Di/+}$:$Cx3cr1^{GFP/+}$ mouse line (Fig. 1A). After tamoxifen treatment, antibody detection of the hemagglutinin (HA) tag fused to the Gi-DREADD receptor was specifically localized to the membrane of green fluorescent protein–positive (GFP^+) microglia, with no detectable expression in $CD206^+$ border-associated macrophages (BAMs), $NeuN^+$ neurons, glial fibrillary acidic protein–positive ($GFAP^+$) astrocytes, or $CC1^+$ oligodendrocytes (Fig. 1, B and C). We then administered the DREADD agonist deschloroclozapine (DCZ, i.p.) to activate microglial Gi-DREADD (*20*). A dose of DCZ (100 μg/kg) takes effect in the brain within 30 min and is eliminated from the body within 24 hours (*20*).

We used in vivo two-photon microscopy to image microglial dynamics in the cortex following Gi-DREADD activation in awake

[1]Department of Neurology, Mayo Clinic, Rochester, MN 55905, USA. [2]Mayo Clinic Graduate School of Biomedical Sciences, Rochester, MN 55905, USA. [3]Center for Neuroimmunology and Glial Biology, Institute of Molecular Medicine, University of Texas Health Science Center at Houston, Houston, TX 77030, USA.
*Corresponding author. Email: longjun.wu@uth.tmc.edu

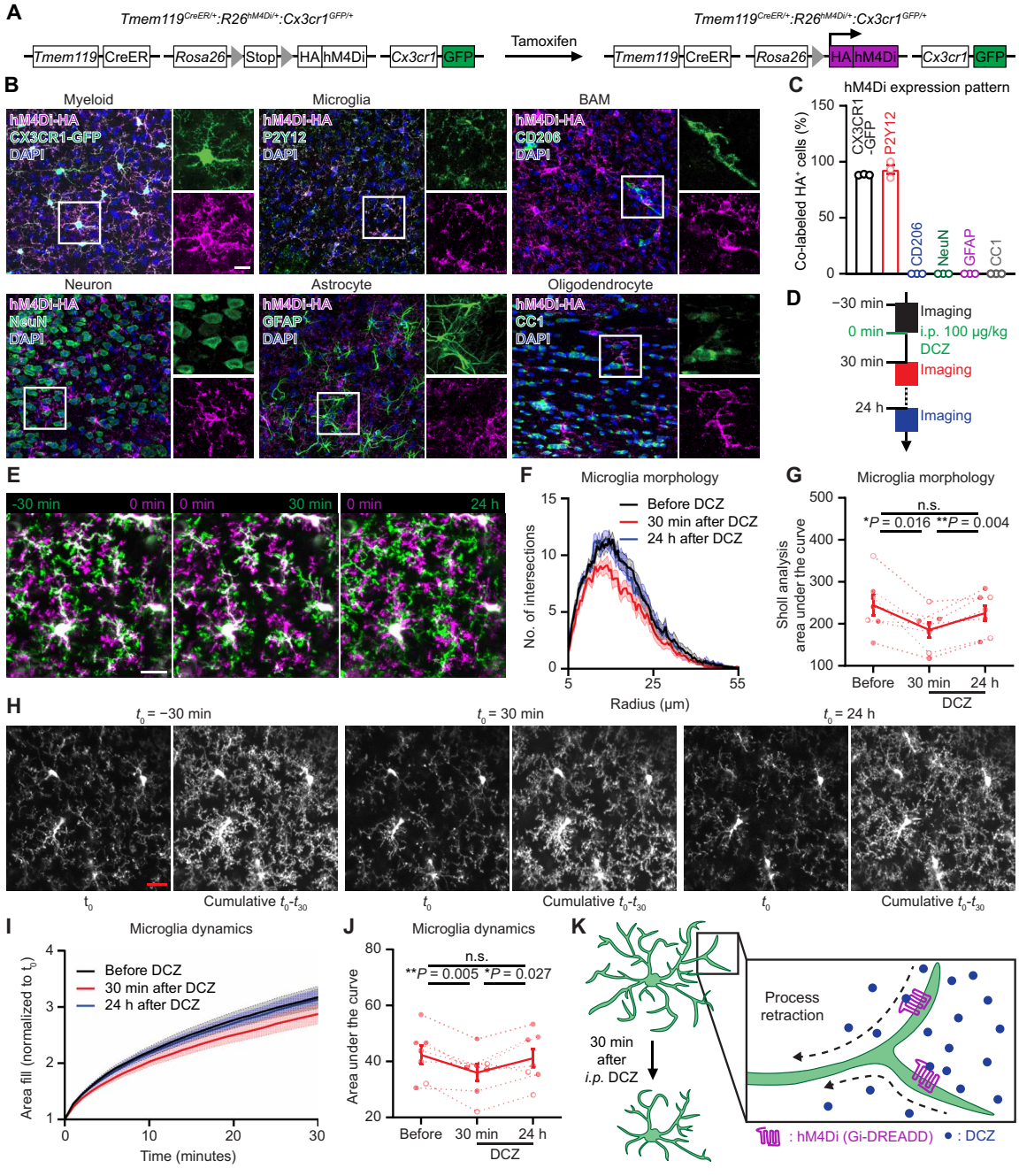

Fig. 1. Microglial Gi signaling reduces microglial process surveillance. (**A**) The genetic strategy used for the expression of hM4Di (Gi-DREADD) and GFP in microglia. (**B** and **C**) Immunostaining (B) and quantification (C, $n = 3$ mice) reveal the membrane localization of HA-tagged hM4Di (magenta) exclusively on microglia (GFP^+ or $P2Y12^+$, green), not on border-associated macrophages (BAMs; $CD206^+$, green), neurons ($NeuN^+$, green), astrocytes ($GFAP^+$, green), and oligodendrocytes ($CC1^+$, green). Scale bar, 10 μm (B). (**D**) Timeline of in vivo two-photon imaging. (**E**) Representative two-photon images illustrate microglial morphology alterations at each study phase. Increased magenta signal area in the mid-panel indicates microglial process retraction 30 min following DCZ injection. Scale bar, 20 μm. (**F** and **G**) Sholl analysis (F) and the area under the curve quantification (G) demonstrate microglial process retraction 30 min postadministration, returning to baseline 24 hours later ($n = 7$ mice). (**H**) Two-photon images show cumulative microglial surveillance at each study phase. Microglia exhibited reduced surveillance area postinjection. Scale bar, 20 μm. (**I** and **J**) Normalized cumulative microglial surveillance area (I) and the area under the curve quantification (J) demonstrate decreased microglial surveillance 30 min postinjection, returning to baseline 24 hours later ($n = 7$ mice). (**K**) Diagram illustrating microglial Gi-DREADD activation leads to microglial process retraction 30 min postadministration. In all graphs, each point indicates an individual mouse (solid: male; hollow: female). Data are represented as the mean ± SEM. Repeated-measures one-way ANOVA followed by a Bonferroni's post hoc test [(G) and (J)]. n.s., not significant; h, hours.

mice. Unexpectedly, we found that systemic DCZ acutely induced microglial process retraction (Fig. 1, D to G, and movie S1), while microglia process extension or retraction speed was not affected (fig. S1, A and B). DCZ-induced microglial process retraction was gradually returned to baseline levels 24 hours later (Fig. 1, D to G). Furthermore, analyses of process dynamics over 30 min showed that microglia survey less area of the cortical parenchyma 30 to 60 min after DCZ injection, compared with baseline and 24 hours after DCZ injection (Fig. 1, H to J). A dose-response study indicated that a lower dosage of DCZ (1 μg/kg) did not lead to alterations in microglia morphology 30 min after injection (fig. S1, C to F). Time-lapse imaging analysis revealed that microglia process retraction peaked 30 min postinjection and began returning to baseline as early as 2 hours postadministration (fig. S1, G and H). Moreover, Gi-DREADD activation did not interfere with endogenous microglial Gi-GPCR functions. Microglia showed similar P2Y12-mediated chemotaxis speed before and after DCZ (100 μg/kg) injection after laser-induced injury (fig. S1, I and J). Together, these results indicate that chemogenetic activation of microglial Gi signaling transiently decreases microglial process surveillance in awake mice (Fig. 1K). As a control, in $Tmem119^{CreER/+}$:$Cx3cr1^{GFP/+}$ mice (fig. S2A), DCZ injection did not alter microglia morphology (fig. S2, B to D) and surveillance area (fig. S2, E to G). Similarly, saline injection in $Tmem119^{CreER/+}$:$R26^{hM4Di/+}$:$Cx3cr1^{GFP/+}$ mice (fig. S2, H and I) also failed to change microglia morphology (fig. S2, J to L) and surveillance area (fig. S2, M to O).

Neuronal activity alters microglial surveillance (*6*, *12*, *21*–*23*). It is possible that DCZ injection indirectly modulates microglial morphology by affecting neuronal activity. To test this possibility, we imaged microglia dynamics in response to DCZ in $Tmem119^{CreER/+}$:$R26^{hM4Di/+}$:$Cx3cr1^{GFP/+}$ mice under anesthesia (fig. S3A). Given that microglia increase surveillance during the first 20 min of anesthesia (*22*, *23*), we initiated imaging microglia 20 min after the anesthesia induction followed by DCZ injection (fig. S3B). Similar to observations in the awake state, chemogenetic activation of microglial Gi signaling induced microglia process retraction (fig. S3, C to E, and movie S2) and decreased microglial process surveillance in anesthetized mice (fig. S3, F to H). In control mice lacking Gi-DREADD expression (fig. S3I), DCZ injection did not affect microglia morphology (fig. S3, J to L) or surveillance area (fig. S3, M to O). These results support the direct role of microglia Gi signaling in reducing microglia process dynamics.

Two-photon microscopy often limits imaging depth to the cortex. We additionally wanted to assess more universal changes in microglial morphology across brain regions following Gi-DREADD activation. To evaluate microglial morphology, we performed Iba1 immunostaining and then used trainable Weka Segmentation to render microglia for Sholl analyses (Fig. 2A) (*24*). Our results suggest that microglia decrease their process length and exhibit less complexity in the cortex (Fig. 2, B to D), corpus callosum (Fig. 2, E to G), and hippocampus (Fig. 2, H to J) when DCZ is administered to Gi-DREADD mice (versus their $Tmem119^{CreER/+}$ genotype controls). In contrast, saline injection did not alter microglial morphology (fig. S4, A to I). Thus, activation of microglial Gi signaling induces process retraction across brain regions.

Activation of microglial Gi signaling reduces microglia-neuron soma interactions

Microglia engage in dynamic intercellular communication through close contact and surveillance of neuronal somata (*7*, *25*). Therefore, we investigated the impact of Gi-DREADD–mediated microglial process retraction on microglia-neuron soma interactions by evaluating the changes in microglial processes proximity to neuronal somata. To visualize these interactions in real time, we injected AAV2/5-CaMKIIa-tdTomato to label excitatory neurons in both $Tmem119^{CreER/+}$:$Cx3cr1^{GFP/+}$ and $Tmem119^{CreER/+}$:$R26^{hM4Di/+}$:$Cx3cr1^{GFP/+}$ mice (Fig. 3A). We then acquired videos before, 0 to 60 min after, and 24 hours after the DCZ injection (Fig. 3B). The DCZ injection in $Tmem119^{CreER/+}$:$Cx3cr1^{GFP/+}$ control mice had no notable effect on microglia-neuron soma interactions (Fig. 3C). However, in $Tmem119^{CreER/+}$:$R26^{hM4Di/+}$:$Cx3cr1^{GFP/+}$ mice, a rapid reduction in microglia surveillance specifically decreases process contact frequency with neuronal somata 30 to 60 min after DCZ administration (Fig. 3, D and E, and movie S3). However, for processes remaining in contact with somata, their duration of interaction was similar to baseline (Fig. 3F). This suggests that certain stable physical interactions might be formed, which appear to be resistant to microglial Gi-DREADD activation. In addition, somatic interaction events by microglia returned to the baseline levels 24 hours post-DCZ injection (Fig. 3E).

Somatic contacts between microglia processes and neuronal somata have been previously characterized as purinergic junctions, involving microglial P2Y12 receptors and neuronal $Kv2.1^{+}$ membrane domains (*7*, *26*). We performed immunostaining of P2Y12 and Kv2.1 to assess the interaction 30 min after the DCZ injection (Fig. 3, G and I). Relative fluorescence intensity around neuronal perimeter quantified neuronal Kv2.1 membrane domains (Kv2.1 $\geq$ 0.3 and P2Y12 $\leq$ 0.3, magenta), nonpurinergic microglial contacts (Kv2.1 $\leq$ 0.3 and P2Y12 $\geq$ 0.3, green), and purinergic junctions (Kv2.1 $\geq$ 0.3 and P2Y12 $\geq$ 0.3, white) (Fig. 3, H and J). We found that both the total microglia-neuron soma interaction and the formation of purinergic junctions decreased in $Tmem119^{CreER/+}$:$R26^{hM4Di/+}$ mice after DCZ treatment (Fig. 3, K and L). No differences were observed in microglial-neuron soma interaction in the saline-injected $Tmem119^{CreER/+}$ and $Tmem119^{CreER/+}$:$R26^{hM4Di/+}$ mice (fig. S4, J to O). These results suggest the microglial Gi signaling–induced process retraction further disrupts microglial interactions with neuronal somata.

In addition, we investigated whether microglia process retraction could also reduce their interactions with somata of astrocytes. To do this, we performed the immunostaining using Iba1 for microglia, and S100β for astrocytes (Fig. 3M) in the cortex. Compared with the control group, mice that received DCZ injection did not exhibit a reduction in interaction with astrocyte somata (Fig. 3N). These results suggest that the process selectively decreases proximity to neuronal somata (Fig. 3O), potentially because astrocytes have fewer baseline interactions with microglia compared to neurons.

Activation of microglial Gi signaling reduces neuronal activity and synchronization

Physical microglia-neuron interactions are closely linked to the regulation of neuronal activity (*2*–*5*). Recent findings have indicated that purinergic junctions formed between microglia processes and neuron somata serve a protective role against neuronal excitotoxicity in stroke (*26*). Here, we used in vivo two-photon calcium imaging (AAV9-CaMKIIa-GCaMP6s) to assess neuronal activity following microglial Gi-DREADD activation (Fig. 4, A and B). In $Tmem119^{CreER/+}$ control mice, DCZ did not alter neuronal activity (Fig. 4C). However, in $Tmem119^{CreER/+}$:$R26^{hM4Di/+}$ mice, we observed a reduction in

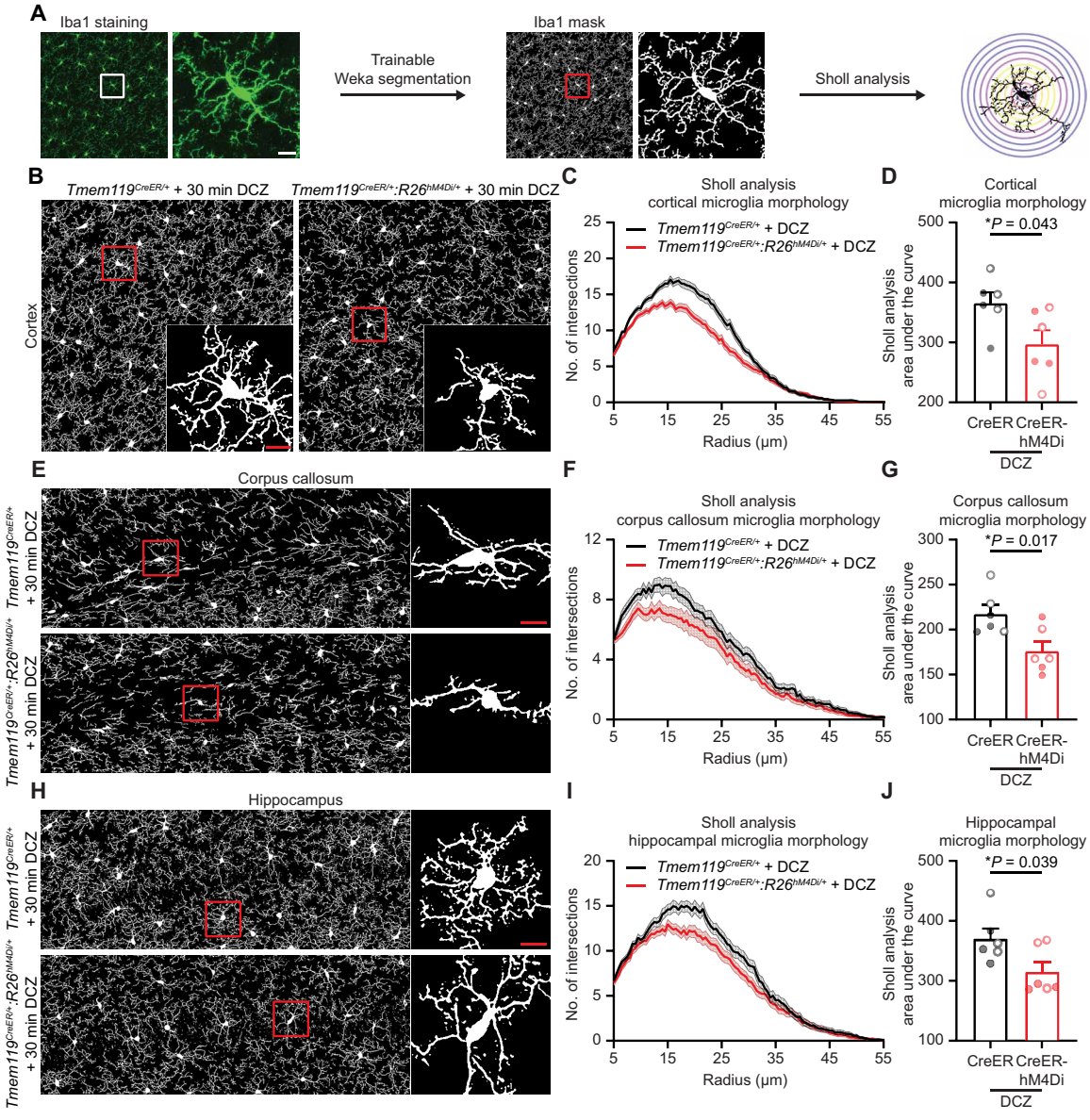

Fig. 2. Microglial Gi-DREADD activation reduces microglia process length in various brain regions. (**A**) Diagram illustrating the data processing. Iba1 immunostaining images were thresholded using trainable Weka segmentation, and microglia were manually selected for Sholl analysis. (**B** to **D**) Analysis of cortical microglia in DCZ-administered control and *Tmem119*$^{CreER/+}$:*R26*$^{hM4Di/+}$ mice. Representative Iba1 mask (B), Sholl analysis (C), and the area under the curve quantification (D) demonstrate process retraction in cortical microglia in *Tmem119*$^{CreER/+}$:*R26*$^{hM4Di/+}$ mice ($n = 6$ mice in each group). (**E** to **G**) Analysis of microglia in the corpus callosum. Representative Iba1 mask (E), Sholl analysis (F), and the area under the curve quantification (G) reveal process retraction in corpus callosum microglia of DCZ-administered *Tmem119*$^{CreER/+}$:*R26*$^{hM4Di/+}$ mice ($n = 6$ mice in each group). (**H** to **J**) Evaluation of hippocampal microglia. Representative Iba1 mask (H), Sholl analysis (I), and the area under the curve quantification (J) show process retraction in hippocampal microglia 30 min after DCZ administration in *Tmem119*$^{CreER/+}$:*R26*$^{hM4Di/+}$ mice ($n = 6$ mice in each group). In all graphs, each point indicates an individual mouse (solid: male; hollow: female). Data are represented as the mean ± SEM. Unpaired *t* test [(D), (G), and (J)]. Scale bars, 10 μm [(A), (B), (E), and (H)].

neuronal active time, signal area, and calcium transient events 30 min after the DCZ injection (Fig. 4, D to G), while the duration of calcium transients remained unaltered (Fig. 4H). Next, we investigated the local neuronal network synchronization using the MATLAB-based Mic2net program (*27*). Neuron connectivity and connectance were calculated to assess the synchronization of neuronal network. We found a decrease in neuronal connectivity and reduced synchronization 30 min after DCZ injection (Fig. 4, I to L). Reduced neuronal activity and synchronization returned to baseline levels 24 hours after DCZ administration (Fig. 4, E to G, K, and L). To exclude the possible effects from unintended Cre-independent Gi-DREADD expression, we assessed the neuronal activity and synchronization alteration in *R26*$^{hM4Di/hM4Di}$ mice following DCZ administration. Strengthening our conclusions, there were no changes in neuronal activity (fig. S5, A to E) or synchronization (fig. S5, F to H) observed 30 min postadministration. These data indicate that

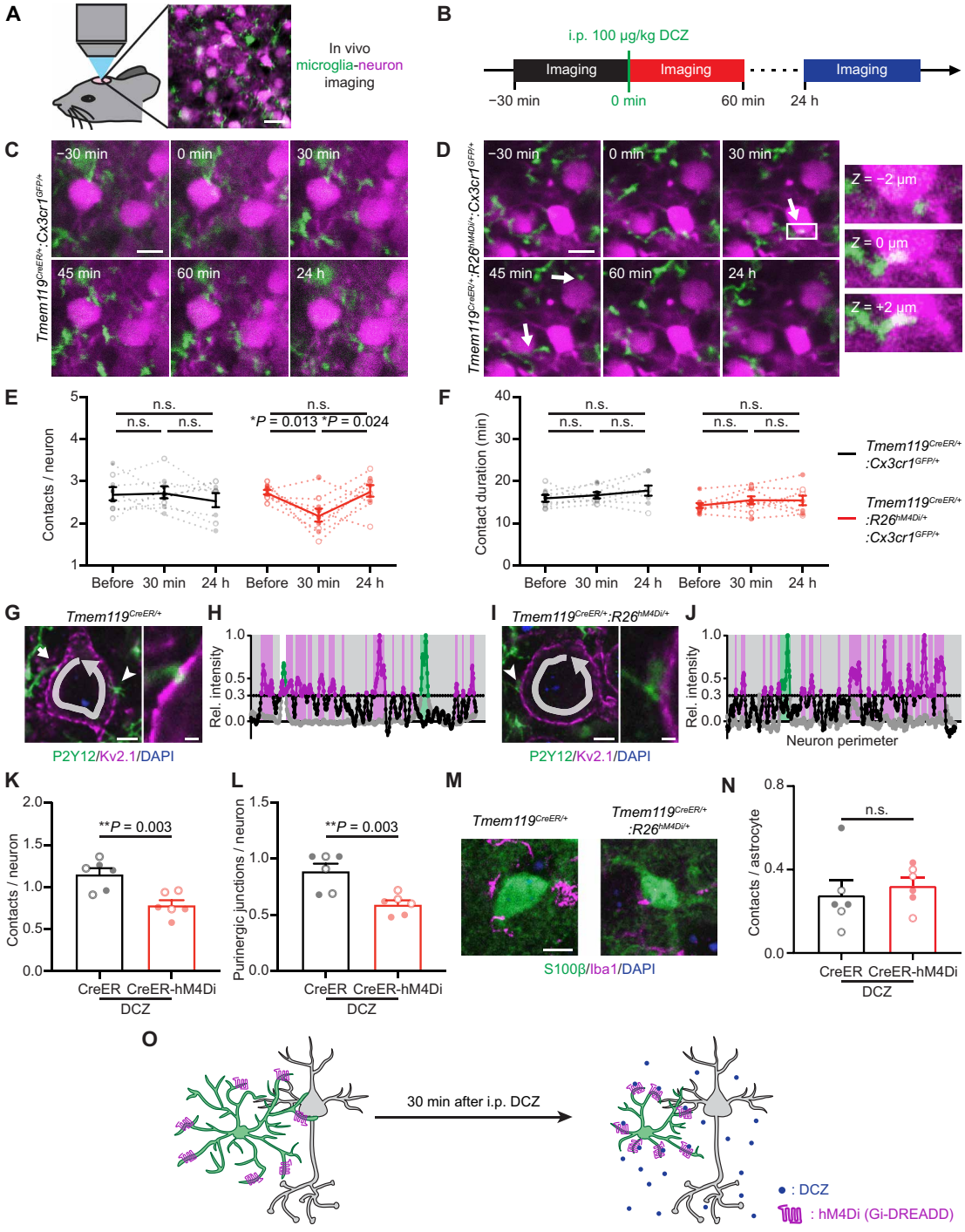

Fig. 3. Activation of microglial Gi signaling decreases microglia-neuron soma interactions. (**A** and **B**) Experimental design diagram (A) and timeline (B) illustrating two-photon imaging of microglia-neuron soma interactions in real-time. Scale bar, 20 μm (A). (**C** to **F**) Time-lapse images [(C) and (D) microglia, green; neuron, magenta] and quantifications of microglia contact number (E) and contact duration (F) reveal fewer contact events 30 to 60 min after Gi-DREADD activation, while the contact duration was unchanged. The interaction number returned to baseline 24 hours later ($n = 8$ mice, *Tmem119*$^{CreER/+}$:*Cx3cr1*$^{GFP/+}$; $n = 9$ mice, *Tmem119*$^{CreER/+}$:*R26*$^{hM4Di/+}$:*Cx3cr1*$^{GFP/+}$). Scale bars, 10 μm [(C) and (D)]. (**G** to **L**) Immunostaining [(G) and (I)], plots of neuron perimeter versus fluorescence intensity [(H) and (J)], and quantifications [(K) and (L)] reveal that microglia processes had fewer total contacts (K) and purinergic junctions (L) per neuron after Gi-DREADD activation ($n = 6$ mice in each group). The arrow indicates the purinergic junction (G), and the arrowheads indicate the nonpurinergic contacts (G and I). Scale bars, 5 μm (left) and 1 μm (right). (**M** and **N**) Immunostaining (M) and quantifications (N) of microglia process (Iba1$^+$, magenta) contacts per astrocyte (S100β$^+$, green) reveals no significant difference between groups ($n = 6$ mice in each group). Scale bar, 5 μm (M). (**O**) Diagram illustrating microglial Gi-DREADD activation decreases contact between microglial processes and neuronal somata. In all graphs, each point indicates an individual mouse (solid: male; hollow: female). Data are represented as the mean ± SEM. Repeated-measures one-way ANOVA followed by a Bonferroni's post hoc test [(E) and (F)]. Unpaired *t* test [(K) to (N)]. n.s., not significant.

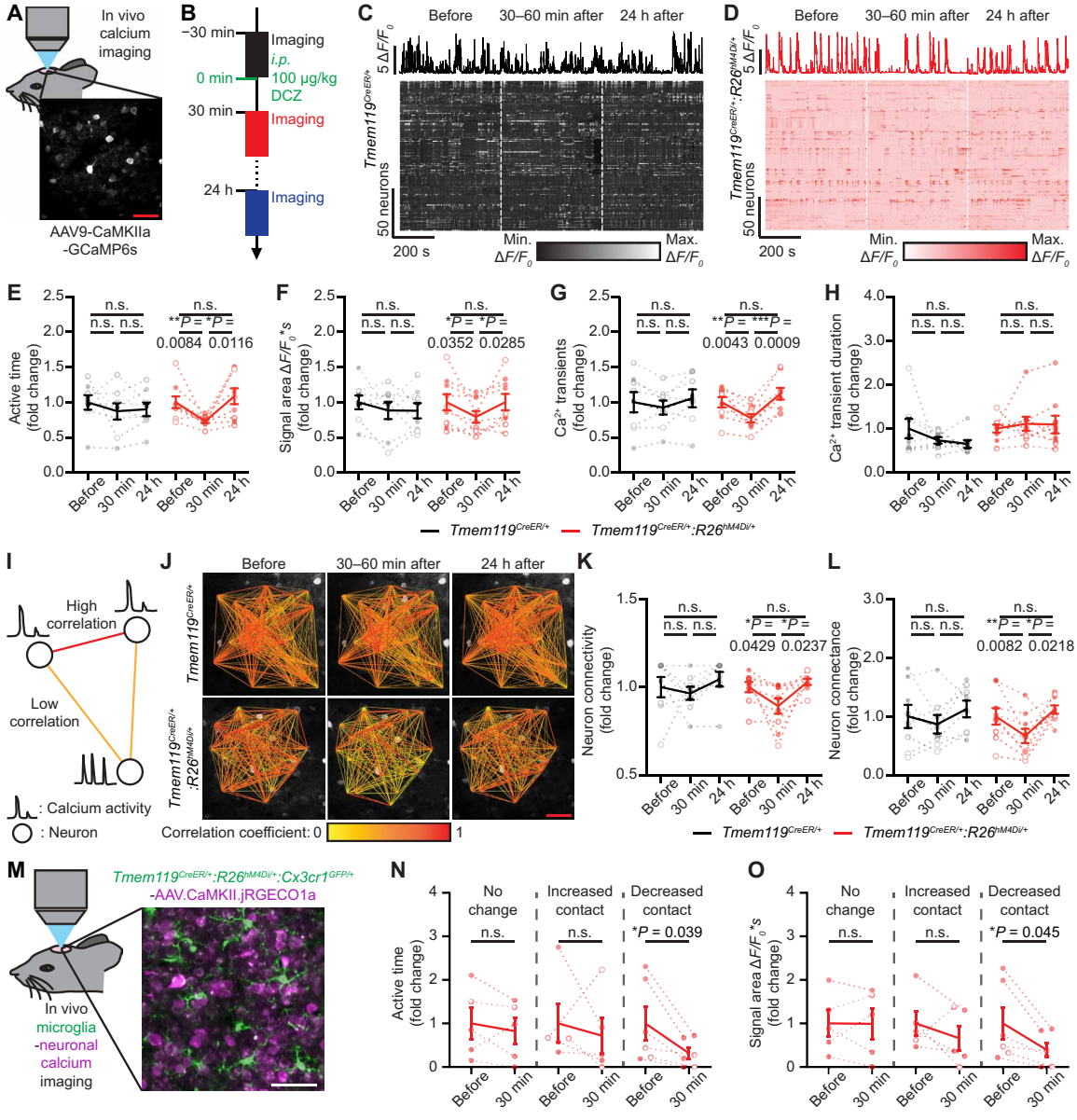

Fig. 4. Microglial Gi-DREADD activation reduces neuronal activity and synchronization. (**A** and **B**) Experimental design (A) and timeline (B) of two-photon imaging for assessing excitatory neuron activity. (**C** to **H**) Single neuronal calcium activity traces (upper) and heatmap of all neuronal calcium activity (lower) in *Tmem119*$^{CreER/+}$ (C) and *Tmem119*$^{CreER/+}$:*R26*$^{hM4Di/+}$ mice (D). Neuronal active time (E), signal area (F), and calcium transient events (G) decreased postinjection in *Tmem119*$^{CreER/+}$:*R26*$^{hM4Di/+}$ mice, recovering 24 hours later. Calcium transient duration was unaffected (H). (**I**) Diagram of calcium activity correlation coefficient analysis (high, red; low, yellow). (**J**) Neuronal network analysis overlaid on calcium images. Fewer red edges in the lower mid-panel suggest the hyposynchronization. (**K** and **L**) Quantifications revealing decreased neuron connectivity (K) and neuron connectance (L) post–Gi-DREADD activation, returning to baseline 24 hours later. (**M**) Diagram illustrating two-photon imaging of GFP^{+} microglia (green) and calcium activity of excitatory neurons (magenta). (**N** and **O**) Neurons categorized by microglia contact changes post-injection. No significant changes in neuronal active time (N) and signal area (O) in increased and no change groups, but a reduction in decreased contact group. ($n = 6$ mice, one mouse lacked neurons in increased contact group, another lacked neuron in no change group.) In all graphs, each point indicates an individual mouse (solid: male; hollow: female). Data are represented as the mean ± SEM. Repeated-measures one-way ANOVA followed by a Bonferroni's post hoc test [(E) to (H), (K), and (L)]. Paired *t* test [(N) and (O)]. n.s., not significant. Scale bars, 50 μm [(A), (J), and (M)]. $n = 8$ mice, *Tmem119*$^{CreER/+}$; $n = 9$ mice, *Tmem119*$^{CreER/+}$:*R26*$^{hM4Di/+}$ [(E) to (H), (K), and (L)].

temporary activation of microglial Gi signaling reduces neuronal activity and synchronization.

To further validate the correlation between microglial contacts and neuronal activity alterations, we performed intracranial injection of AAV-CaMKII-jRGECO1a to simultaneously visualize neuronal activity and microglia-neuron soma interaction in *Tmem119*$^{CreER/+}$:*R26*$^{hM4Di/+}$:*Cx3cr1*$^{GFP/+}$ mice (Fig. 4M). Imaging of the same field of view was conducted both before and 30 min after DCZ injection. Neurons were categorized into three groups on the basis of postinjection changes in microglia contact: increased contact, decreased contact, and no change. Neuronal activity was then compared within each group. The result indicated no notable changes in neuronal

activity in the increased contact or no change groups. However, neuronal activity was substantially reduced in the decreased contact group (Fig. 4, N and O). This detailed cellular evidence supports our hypothesis that decreased contact between microglia and neuronal somata correlates with reduced neuronal activity.

Despite Tmem119 being predominantly expressed in microglia in the central nervous system, its expression in peripheral cell types necessitated additional verification that the observed reductions in neuronal activity and synchronization were indeed caused by microglial Gi signaling (Fig. 5, A and B). The query of the RNA sequencing database demonstrates that the combination of genetic microglia manipulation (Tmem119 driven) and pharmacological microglia ablation (targeting CSF1R) effectively narrowed the cell population to microglia (Fig. 5B). Therein, we ablated microglia through PLX3397 administration, a CSF1R inhibitor, to alleviate the off-target concern. If the reduced neuronal activity after DCZ injection was dependent on microglia, we should rescue the phenotype after microglia ablation. When PLX3397 chow was provided 2 weeks before the calcium imaging (Fig. 5, C to E), we did not observe the previously noted reductions in neuronal active time, signal area, or calcium transient events (Fig. 5, F to J). In addition, there were no alterations in the local neuronal connectivity or synchronization 30 min following the DCZ injection (Fig. 5, K to M). These results strongly support that activation of microglia

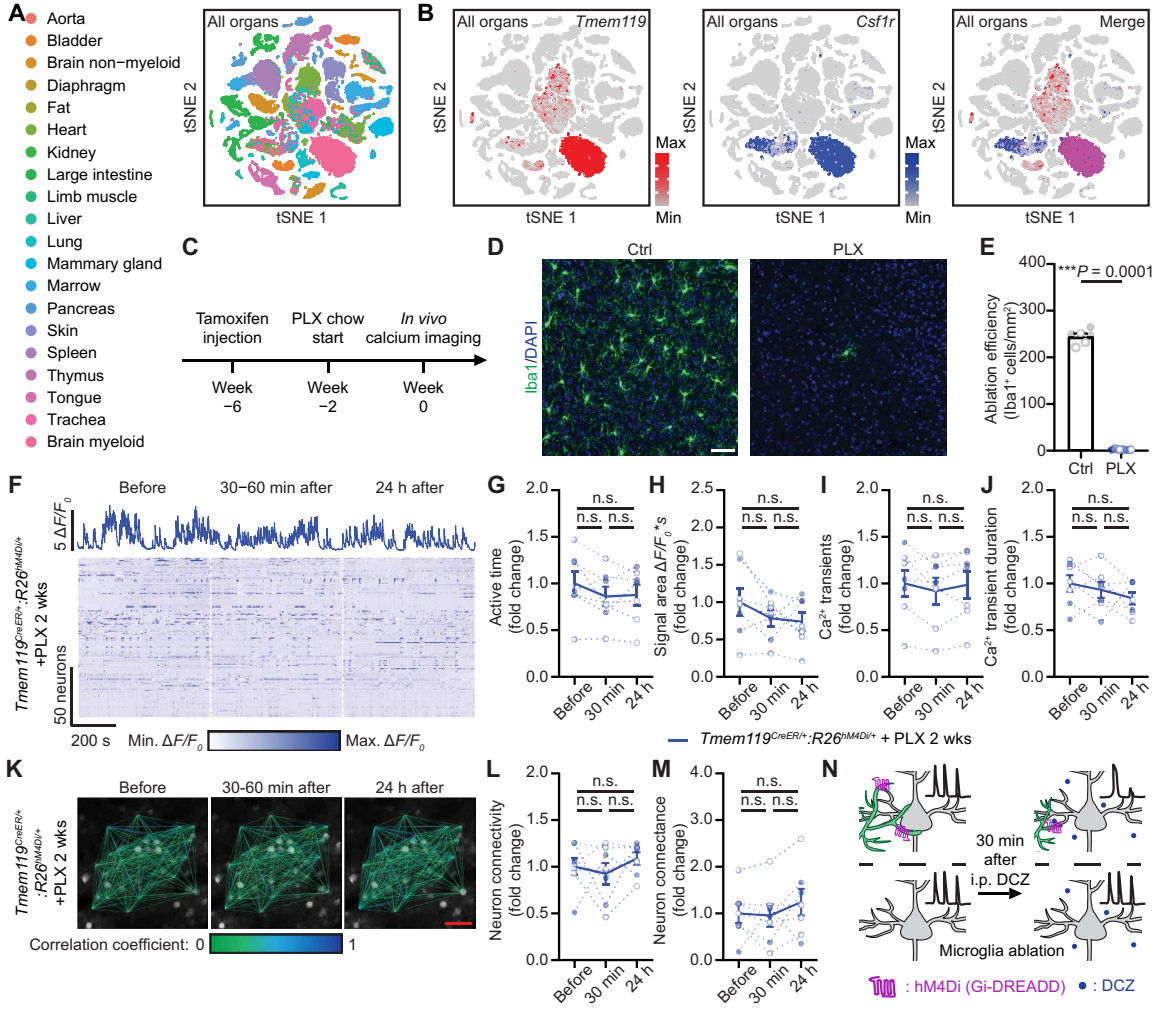

Fig. 5. Microglia ablation rescues microglial Gi signaling–induced neuronal hypoactivity and hyposynchronization. (**A** and **B**) Query of Tabula Muris database showing cells in 20 mouse organs (A) demonstrating the dense expression of *Tmem119* and *Csf1r* in brain myeloid cells and sparse detection in other peripheral organs (B). (**C**) Timeline depicting the induction of Gi-DREADD expression, microglia ablation, and in vivo two-photon calcium imaging. (**D** and **E**) Representative images (D) and quantitative analysis (E) demonstrating efficient microglia ablation (Iba1$^+$, green) in the brain with PLX treatment ($n = 6$ mice in each group). Scale bar, 50 μm. (**F** to **J**) Single neuronal calcium activity traces (upper) and heatmap of all neuronal calcium activity (lower) at each study phase (F). Quantifications reveal no alteration in neuronal active time (G), signal area (H), calcium transient events (I), and calcium transient duration (J) after the DCZ injection ($n = 7$ mice in each group). (**K** to **M**) Representative neuronal network analysis plotted on top of two-photon calcium images in microglia ablated *Tmem119*$^{CreER/+}$:*R26*$^{hM4Di/+}$ mice at each study phase (K). Quantifications reveal unaltered neuron connectivity (L) and neuron connectance (M) after the DCZ injection in microglia ablated *Tmem119*$^{CreER/+}$:*R26*$^{hM4Di/+}$ mice ($n = 7$ mice in each group). Scale bar, 50 μm. (**N**) Diagram illustrating microglial Gi-DREADD activation reduces neuronal activity, and microglia ablation rescues Gi-DREADD induced neuronal hypoactivity. In all graphs, each point indicates an individual mouse (solid: male; hollow: female). Data are represented as the mean ± SEM. Unpaired *t* test (E). Repeated-measures one-way ANOVA followed by a Bonferroni's post hoc test [(G) to (J), (L), and (M)]. n.s., not significant.

Gi signaling truly reduced neuron activity and synchronization (Fig. 5N).

DISCUSSION

In this study, we combined microglial chemogenetics with in vivo two-photon imaging to investigate the impact of microglial Gi signaling in the regulation of neuronal function. Upon activation of microglial Gi signaling, we observed decreased microglial surveillance, reduced neuronal activity, and impaired local neuronal synchrony. The altered neuronal functions were associated with a decrease in microglial process interaction with neuronal somata. While there are concerns about specificity of $R26^{hM4Di/hM4Di}$ mouse line, we have previously demonstrated that mCitrine leakage is not associated with Gi-DREADD expression (*15*). DCZ did not reduce neuronal activity in $Tmem119^{CreER/+}$:$R26^{hM4Di/+}$ mice when microglia were ablated, nor in $R26^{hM4Di/hM4Di}$ homozygous mice. Microglial ablation not only eliminates potential off-target effects from neurons but also rules out possible contributions from other $Tmem119^{+}$ cells. If there was leaky expression of Gi-DREADD in neurons, microglial ablation would not be able to abolish the effect of DCZ on neuronal activity, which is not the case in the current study. Collectively, these findings suggest that microglia Gi signaling can transiently modulate neuronal activity through physical interactions with neurons in the homeostatic brain.

Regulation of microglial process dynamics by Gi signaling pathway

Microglia express a number of Gi-GPCRs, such as CX3CR1, P2Y12, and C3aR (*28*). Previous studies have shown that the microglia Gi signaling pathway governs the microglial process functions, including chemotaxis and dynamic movement. Specifically, P2Y12 and C3aR are known to mediate microglial process chemotaxis (*29*, *30*). The absence of CX3CR1 leads to reduced microglia process length (*31*). Furthermore, suppressing Gi signaling in microglia via selective PTX expression resulted in shorter and less dynamic microglial processes (*13*). These varied consequences of inhibiting microglial Gi-GPCR underscore the importance of the Gi signaling pathway in regulating microglial process morphology and motility.

In our study, we used chemogenetic manipulation to selectively activate microglial Gi signaling, which led to a reduction in microglial process length and a decrease in surveillance. In addition, this effect is transient, with microglial morphology and surveillance returning to baseline levels 24 hours after DCZ injection. Together with previous reports, these observations suggest a "U-shaped" regulatory function by the microglial Gi signaling on microglia dynamics, where both increased and decreased Gi signaling can lead to lower microglial surveillance.

Microglial calcium activity may play a central role in this "U-shaped" regulation of neuronal activity via Gi signaling. Recent evidence indicates that microglial calcium levels are associated with process extension (*32*), and activating Gi-DREADD has been shown to increase microglial calcium activity (*33*). Combining with our findings of retracted microglial processes following Gi-DREADD activation, these results suggest that both microglia process extension and retraction are linked to elevated calcium levels. In addition, activation of microglial P2Y12 receptors has been shown to increase microglial calcium levels, supporting the role of microglial Gi-GPCRs in calcium regulations (*33*, *34*). Although the specific effects of inhibiting microglial Gi signaling pathway on intracellular calcium remain unclear, previous studies have shown that elevated cyclic adenosine 5′-monophosphate (cAMP) can trigger calcium release from endoplasmic reticulum by sensitizing inositol 1,4,5-trisphosphate–gated ion channels (*35*, *36*). Therefore, it is possible that both activation and inhibition of microglial Gi-GPCRs could lead to process retraction by increasing intracellular calcium.

Furthermore, the microglial morphology alteration may stem from the reorganization of the cytoskeleton, involving filamentous actin (F-actin) or microtubules. Activation of Gi-GPCR results in cAMP down-regulation, which leads to the decompartmentalization of F-actin and the subsequent collapse of microglial filopodia (*37*). In addition, Gi-GPCR is implicated in the microtubule dynamics (*38*). Small Gi proteins are able to inhibit microtubule assembly by interacting with the GTP cap of growing microtubules (*39*), offering an alternative mechanism by which Gi-DREADD activation could attenuate microglia surveillance. However, these hypotheses need further experiments to confirm.

Last but not least, as of now, there are no established methods for selectively and temporally manipulating microglia morphology in vivo. Our findings that microglial Gi-DREADD activation can transiently decrease surveillance may open up an important avenue for understanding the function of microglial dynamics in neural circuits.

Physical microglia-neuron interactions in the regulation of neuronal functions

Previous studies have demonstrated that genetic knockout of endogenous microglial Gi-GPCRs, like P2Y12, leads to increased anxiety and decreased seizure severity in mice (*6*, *10*–*12*, *40*). Moreover, inhibition of Gi signaling in microglia has been associated with increased neuronal activity and synchronization (*13*). In line with these findings, our current study shows that the chemogenetic activation of microglial Gi signaling reduces neuronal activity and disrupts the local synchronization of neural networks. This is supported by a recent study showing that microglial Gi-DREADD activation induces neuronal hypoactivity, decreases norepinephrine release, and promotes sleep (*33*). Thus, microglial Gi signaling is able to suppress neuronal activity in the homeostatic brain.

Reduced neuronal activity after microglial Gi activation was correlated with fewer interactions between microglia processes and neuronal somata. These interactions are thought to represent a novel method of neuromodulation (*4*, *5*). For instance, during a stroke or seizure, microglial processes could be attracted by the overactive neuron, forming somatic interactions to prevent excitotoxicity (*12*, *26*). Our findings imply that in a nonpathological state, microglia-neuron interactions might actually enhance neuronal activity. Consistent with this, our recent study demonstrated that microglia extended their processes to shield inhibitory synapses on neuronal somata, thereby promoting postanesthesia neuronal activity (*7*). Therefore, it is possible that microglial Gi-DREADD–mediated surveillance down-regulation could disrupt the shielding of inhibitory synapses on neuronal somas, leading to reduced neuronal activity.

Beyond these microglia-neuron soma interactions, microglia are also known to contact with excitatory synapses. An earlier study has shown that microglial contacts with dendritic spines increase spine calcium activity, thereby enhancing the activity of the local neuronal network (*41*). Thus, reduced microglial surveillance might also decrease interactions with excitatory synapses, potentially reducing neuronal activity.

Microglial Gi signaling as a potential target for neuromodulation in health and disease

Recent studies have highlighted the integral role of microglia in the regulation of neuronal activity and synaptic plasticity, such as learning and memory (*42*, *43*), sleep (*44*–*46*), anxiety-like behaviors (*10*), compulsive behaviors (*47*), alcohol intake (*48*), pain (*49*), and seizures (*50*). Beyond direct physical interactions with neurons, these studies suggest alternative regulatory mechanisms whereby microglia release soluble factors and phagocytose extracellular matrix (ECM) to modulate neuronal activity (*51*). Microglia Gi-GPCRs were reported to participate in the regulation of neuronal functions. For example, pharmacologically inhibiting P2Y12 has been shown to prevent ketamine-induced ECM loss (*52*). Thus, the activation of microglial Gi-DREADD might share similar mechanisms to modulate neuronal activity.

While Gi signaling canonically suppresses intracellular cAMP levels and inhibits associated pathways, emerging evidence indicates that microglial Gi signaling can also elevate microglial calcium activity (*33*, *53*). Microglial calcium activity is attuned to neuronal activity (*32*) and is implicated in the release of soluble factors (*54*, *55*) and in enhancing phagocytosis (*34*, *56*). A recent study demonstrated that microglial calcium elevation via Gq-DREADD activation increased the release of interleukin-6 and prostaglandin E_2 from microglia, which subsequently reduced neuronal activity (*57*). Therefore, Gi signaling–mediated calcium elevation might trigger the release of soluble factors and facilitate the phagocytosis of ECM to modulate neuronal activity and network synchronization.

Moreover, microglia Gi signaling can also be potential targets for neuromodulation in neurological diseases. Recent findings indicate that chemogenetic activation of microglia Gi-GPCRs could ameliorate seizures and relieve pain (*16*, *58*). Chronic activation of Gi-DREADD has been shown to reduce the release of pro-inflammatory cytokines and alleviate neuropathic pain (*18*, *19*, *59*, *60*). In the kainic acid–induced seizure model, acute activation of microglial Gi-DREADD reduced neuronal hyperactivity, while chronic activation resulted in neuronal death, suggesting the balance maintained by microglia Gi signaling in the neuromodulation (*17*). Although further research is needed to elucidate the detailed mechanism by which microglial Gi signaling modulates neuronal function, our study identifies microglia Gi signaling as an intriguing target to fine-tune neuronal activity under physiological and pathological conditions.

MATERIALS AND METHODS

Animals

The *Tmem119*$^{CreER/CreER}$ (C57BL/6-Tmem119$^{em1(cre/ERT2)Gfng}$/J, 031820), *R26*$^{hM4Di/hM4Di}$ (B6.129-*Gt(ROSA)26Sor*$^{tm1(CAG-CHRM4*,-mCitrine)Ute}$/J, 026219), and *Cx3cr1*$^{GFP/GFP}$ (B6.129P2(Cg)-*Cx3cr1*^{tm1Litt}/J, 005582) mouse lines were acquired from the Jackson Laboratory and subsequently bred at Mayo Clinic. Tamoxifen (Sigma-Aldrich, 150 mg/kg, i.p.) was administered to all adult mice four times every 2 days to induce Cre-Lox recombination or serve as controls. All experiments were performed at least 4 weeks after tamoxifen injections. Both male and female mice were included in the studies. Mice were housed in a 12-hour light/dark cycle and climate-controlled environment, with ad libitum access to food and water. All experimental procedures (A00002290-16-R22 and A00002731-17-R23) were approved by the Mayo Clinic's Institutional Animal Care and Use Committee.

Cranial window surgeries and virus injections

In preparation for cranial window surgeries, mice were provided with ibuprofen (0.2 mg/ml) in their drinking water for 3 days prior. Anesthesia was induced with 3% isoflurane in oxygen, followed by maintenance at 1.5% in oxygen during surgery. Throughout the surgery, mice were kept on a heating pad. After cutting the skin to expose the skull, a craniotomy was performed to create a circular 4-mm-diameter window above the somatosensory cortex [centered at anteroposterior (AP): −2.0; and mediolateral (ML): +1.5]. Subsequently, a sterile 5-mm glass coverslip (Warner Instruments) was implanted and affixed with dental cement (Tetric EvoFlow). The remaining skull was covered with iBond Total Etch glue (Heraeus) and cured with an LED Curing Light. Additional dental cement (Tetric EvoFlow) was again applied around the glass coverslip and cured. A custom-made head plate was then secured to the window using dental cement. Following the surgery, mice recovered under a heating lamp before being returned to their home cage, receiving ibuprofen (0.2 mg/ml) in their drinking water for an additional 3 days.

For experiments requiring virus injections, after the craniotomy, AAVs were injected into the somatosensory cortex (AP: −2.0; and ML: +1.5) using a microsyringe (Hamilton) and a glass pipette. During the virus injection, the exposed brain surface was kept moist with sterile phosphate-buffered saline (PBS). AAV2/5.CaMKII.tdTomato (Neurophotonics, 661-aav5) was used to label excitatory neurons and AAV9.CaMKII.GCaMP6s.WPRE.SV40 (Addgene, 107790) or AAV2/9.CaMKII.jRGECO1a.WPRE.hGH.polyA (BrainVTA, PT3349) was used to image excitatory neuronal calcium activity. AAVs (300 nl) were injected to target layer II/III neurons [dorsoventral (DV): −0.3, 200 nl, 40 nl/min; and DV: −0.2, 100 nl, 20 nl/min) with a 5-min period for virus diffusion.

Two-photon imaging

Before data acquisition, mice recovered for at least 4 weeks postsurgery and underwent a 3-day training period. During the training session, each mouse spent 1 hour per day on an air-lifted platform (NeuroTar) while being head-fixed under a two-photon microscope (Scientifica). The two-photon microscope was equipped with a Mai-Tai DeepSee laser (Spectra Physics) tuned to 940 nm. A 16× water immersion lens (Nikon) was used, and digital magnification (zoom 5-8) was applied based on experimental requirements. GFP and GCaMP6s signals passed through a 525/50 filter (Chroma), and tdTomato signal passed through a 630/75 filter (Chroma). Laser power was maintained at 6 mW or below.

Imaging in the somatosensory cortex was conducted 50 to 150 μm beneath the pial surface for microglia dynamics (20-μm-thick z-stacked images, once per minute, 2 μm step size, 1024 × 1024 pixels) or 150 to 300 μm for imaging microglia-neuron interactions (20-μm Z-stacked images, 2 μm step size, once per minute, 1024 × 1024 pixels) and neuronal activity (1 Hz frame rate, 512 × 512 pixel resolution). Unless specifically stated, 30-min videos were acquired before, 30 to 60 min, and 24 hours after DCZ injection (100 μg/kg; MedChemExpress). For imaging microglia dynamics in anesthetized mice, the mouse was induced with 3% isoflurane and was then maintained at 1.5% isoflurane for the anesthesia imaging. Under anesthesia, mice were placed on a heating pad (Physitemp) to maintain body temperature at 37°C. Twenty minutes after the anesthesia induction, microglia dynamics images were acquired before and after DCZ injections. For laser-induced injury, the laser was focused at 99× magnification and held at

maximum laser power at an 800-nm wavelength until an autofluorescence spot appeared.

Immunofluorescence staining

Isoflurane anesthetized mice underwent transcardial perfusion with 40 ml of PBS followed by 40 ml of cold 10% formaldehyde in PBS (LabChem). The whole brain was harvested, immersed in 10% formaldehyde overnight at 4°C, and cryoprotected in 30% sucrose in PBS for a minimum 48 hours before cryosectioning. Free-floating sections (30 μm) were obtained using a cryostat (Leica). For immunostaining, sections were rinsed three times in the tris-buffered saline (TBS), blocked with TBS buffer containing 5% donkey serum and 0.4% Triton X-100 at room temperature for 1 hour. Subsequently, they were incubated overnight at 4°C with primary antibodies: rabbit anti-HA (1:200, Cell Signaling Technology, 3724S), chicken anti-GFP (1:1000, Aves Labs, GFP-1010), rat anti-P2Y12 (1:100, BioLegend, 848002), rat anti-CD206 (1:250, Bio-Rad, MCA2235), mouse anti-NeuN (1:500, Abcam, Ab104224), mouse anti-GFAP (1:500, Cell Signaling Technology, 3670S), mouse anti-CC1 (1:200, MilliporeSigma, OP80), rabbit anti-S100β (1:500, Abcam, Ab52642), rabbit anti-Iba1 (1:1000, Abcam, Ab178847), guinea pig anti-Iba1(1:1000, Synaptic Systems, 234308), and mouse anti-Kv2.1 (1:500, antibodies-online Inc., ABIN1304762). Afterward, sections were washed with TBS three times and incubated with donkey secondary antibodies (1:500, Alexa-Fluor 488/594/647 anti-rabbit, anti-mouse, or anti-rat, Invitrogen; A21202, A21207, A21209, A31573, and A32787; or 1:500, Alexa-Fluor 488 anti-chicken and Alexa-Fluor 594 anti-guinea pig, Jackson ImmunoResearch, 703-545-155 and 706-585-148) in blocking buffer for 120 min at room temperature. After three additional washes, sections were mounted with DAPI Fluoromount-G mounting medium (SouthernBiotech). Fluorescent images were acquired using a laser scanning confocal microscope (LSM 980, Zeiss). Ten-micrometer Z-stacked images were obtained by a 20×, 40×, or 63× objective based on experimental requirements. Image brightness and contrast adjustments were made by ImageJ (National Institutes of Health).

Microglial ablation

Microglial ablation was achieved through the administration of a chow containing the colony-stimulating factor 1 receptor (CSF1R) inhibitor, PLX3397 (600 mg/kg, Chemgood), provided ad libitum for a minimum of 2 weeks to ensure complete depletion of microglia. The efficiency of microglial ablation was evaluated through immunostaining of brain sections.

Microglial dynamics, morphology, and process speed analyses

Two-photon z-stacked and time-lapse images were aligned using the ImageJ plug-in, StackReg, to correct any image shifts. For the analysis of microglia dynamics in two-photon images, the cumulative area occupied by microglia was quantified over time. First, a z-projected image was thresholded using the Li method in ImageJ. Cumulative maximum projections of the microglial signal from time (t_x) and previous time points ($t_0 + t_1 + \ldots + t_x$) were generated, and the area filled by the microglial signal was calculated from the beginning (t_0) to the end of the imaging session ($t_0 + t_1 + \ldots + t_{30}$). Subsequently, the data were normalized to the area filled at "t_0" to obtain a relative area surveyed over time, independent of the initial microglia morphology.

For the analysis of microglia morphology from two-photon images, a z-projected image was thresholded using the Li method in ImageJ. All microglia with clear soma were manually selected for Sholl analysis. In addition, to analyze microglia morphology from Iba1 immunostaining, a z-projected image was initially segmented using the trainable Weka Segmentation plug-in in ImageJ. Subsequently, 10 to 15 microglia per mouse were randomly selected for Sholl analysis.

For the analysis of microglia process speed in two-photon images, primary branch movements were manually traced using Manual Tracking plug-in in ImageJ. To compare microglia process movement speed before and after DCZ injection, at least three extending and three retracting primary branches were measured per microglia. For the comparison of microglial chemotaxis speed pre- and post-DCZ injection, at least 10 processes per field of view were analyzed.

Microglia-neuron soma interaction analyses

Two-photon Z-stacked time-lapse images were aligned using the ImageJ plug-in, HyperStackReg, to correct any image shifts. To quantify in vivo interactions between neuronal somata and microglial processes, three planes of two-photon images (4 μm thick) were average projected. A segmented line (1.5 μm wide) was then drawn along the neuron soma. Subsequently, the "Plot Profile" tool was used to profile the GFP fluorescence intensity (representing microglia processes) along the tdTomato$^+$ neuron soma. All neurons with clear soma were included in the analysis, excluding those interacting with microglia soma. The raw fluorescence intensity was converted into $\Delta F/F_0$, where F_0 was defined as the 50th percentile value for each neuron. Next, all $\Delta F/F_0$ values were normalized by the maximum $\Delta F/F_0$ observed across all analyzed neurons in this time-lapse average projected image. Instances with a relative $\Delta F/F_0 > 0.3$ for more than 0.5 μm were considered as interaction events. The number of interaction events during the 30-min imaging period and the contact duration were then calculated.

For the analysis of microglia-neuron/astrocyte soma interaction in immunostaining images, a segmented line (1.5 μm wide) was drawn along the Kv2.1$^+$/S100β$^+$ neuron/astrocyte soma. A single plane of confocal images was split into a Kv2.1/S100β channel and a P2Y12/Iba1 channel. Similar to the two-photon image analysis, the "Plot Profile" tool was used to profile identical segmented lines in each channel. F_0 was defined as the 5th percentile value for Kv2.1 and the 50th percentile value for P2Y12/Iba1. Data processing steps were the same as the analysis of microglia-neuron soma interaction in two-photon images. Thirty to 50 neurons per mouse were randomly selected for this analysis.

Neuronal calcium imaging analyses

Two-photon time-lapse images underwent registration using the ImageJ plug-in, TurboReg, to correct any image shifts. For the analysis of neuronal calcium activity, an average intensity image of the entire video was generated to facilitate the selection of neuron somata. Neuron somata were manually drawn using the oval selection tool. Neurons lacking "donut-shaped" calcium activity were excluded from the analysis. Then, mean fluorescent intensity values were obtained and subsequently converted into $\Delta F/F_0$. The baseline fluorescence was defined as the lower 25th percentile value across all frames. Neurons exhibiting $\Delta F/F_0 > 0.25$ were

considered "active." Parameters such as neuronal active time, signal area, and calcium transient events and duration were calculated accordingly.

To evaluate the neural network synchronization, time-lapse calcium imaging data were analyzed using the MATLAB-based Mic2net program (*27*). Mic2net algorithms provide automated processing and quantitative assessment of neuronal calcium imaging data that has been preprocessed using ImageJ. Cross-correlation analysis was used to determine the synchronization between pairs of neurons. To rule out insignificant correlations, cutoff values were determined using a scrambled dataset. This set was generated by shuffling the time series of calcium imaging to random starting points. The 99th percentile of the cross-covariance values from the scrambled dataset was then applied as the cutoff value. Connectivity was defined as the number of neurons exhibiting a correlation coefficient higher than the cutoff, divided by the total number of neurons. Connectance, on the other hand, was defined as the number of significant edges divided by the maximum possible number of edges in the network, providing a quantitative measure of the overall network synchronization.

Single-cell RNA sequencing database queries

The Tabula Muris database served as the resource for determining *Tmem119* and *Csf1r* expression across 20 mouse organs at the single-cell level (*61*). All indexed R objects (https://figshare.com/articles/dataset/Robject_files_for_tissues_processed_by_Seurat/5821263) were updated to the newest Seurat version 4.0 object (*62*) using the UpdateSeuratObject function. These objects were then combined into one Seurat object using the merge function. Normalization of gene counts was performed by NormalizeData function. The data were further scaled by ScaleData function. Highly variable features were called by FindVariableFeatures function. Initial dimensionality reduction was carried out via principal components analysis, followed by t-distributed stochastic neighbor embedding (tSNE). Visualization of the results was achieved using Dimplot for tSNE plots. FeaturePlot function was used to illustrate *Tmem119* and *Csf1r* expression levels.

Statistics

Detailed statistical information, including sample size and statistical methods, is provided in the figure legends corresponding to each specific experiment. In general, normality was first assessed, and all data followed the Gaussian distribution. An unpaired two-tailed *t* test was used for comparing experiments involving two groups. In instances where two time points from the same animal were compared, a paired two-tailed *t* test was used. For comparisons with more than two time points from the same animal, repeated-measures one-way analysis of variance (ANOVA) was performed, followed by a Bonferroni's post hoc analysis for multiple comparisons. Results are presented as the mean ± SEM, and statistical significance was determined when $P < 0.05$. Statistical analyses were performed using GraphPad Prism 10 software. Experimental designs and sample sizes were determined to minimize animal usage and distress while ensuring sufficiency for detecting robust effect sizes. Researchers were aware of genotypes and treatments during experiments and data analysis. To mitigate potential bias, we implemented rigorous controls and automated data analysis wherever possible. These analysis steps are detailed in Materials and Methods to ensure transparency and reproducibility of our findings. All experiments were at least replicated twice in laboratory.

Supplementary Materials

The PDF file includes:
Figs. S1 to S5
Legends for movies S1 to S3

Other Supplementary Material for this manuscript includes the following:
Movies S1 to S3

REFERENCES AND NOTES

1. S. A. Wolf, H. W. Boddeke, H. Kettenmann, Microglia in physiology and disease. *Annu. Rev. Physiol.* **79**, 619–643 (2017).
2. H. Wake, A. J. Moorhouse, A. Miyamoto, J. Nabekura, Microglia: Actively surveying and shaping neuronal circuit structure and function. *Trends Neurosci.* **36**, 209–217 (2013).
3. S. Zhao, A. D. Umpierre, L. J. Wu, Tuning neural circuits and behaviors by microglia in the adult brain. *Trends Neurosci.* **47**, 181–194 (2024).
4. A. D. Umpierre, L. J. Wu, How microglia sense and regulate neuronal activity. *Glia* **69**, 1637–1653 (2021).
5. B. S. Whitelaw, M. B. Stoessel, A. K. Majewska, Movers and shakers: Microglial dynamics and modulation of neural networks. *Glia* **71**, 1575–1591 (2023).
6. A. Badimon, H. J. Strasburger, P. Ayata, X. Chen, A. Nair, A. Ikegami, P. Hwang, A. T. Chan, S. M. Graves, J. O. Uweru, C. Ledderose, M. G. Kutlu, M. A. Wheeler, A. Kahan, M. Ishikawa, Y. C. Wang, Y. E. Loh, J. X. Jiang, D. J. Surmeier, S. C. Robson, W. G. Junger, R. Sebra, E. S. Calipari, P. J. Kenny, U. B. Eyo, M. Colonna, F. J. Quintana, H. Wake, V. Gradinaru, A. Schaefer, Negative feedback control of neuronal activity by microglia. *Nature* **586**, 417–423 (2020).
7. K. Haruwaka, Y. Ying, Y. Liang, A. D. Umpierre, M. H. Yi, V. Kremen, T. Chen, T. Xie, F. Qi, S. Zhao, J. Zheng, Y. U. Liu, H. Dong, G. A. Worrell, L. J. Wu, Microglia enhance post-anesthesia neuronal activity by shielding inhibitory synapses. *Nat. Neurosci.* **27**, 449–461 (2024).
8. K. Cao, L. Qiu, X. Lu, W. Wu, Y. Hu, Z. Cui, C. Jiang, Y. Luo, Y. Shao, W. Xi, L. H. Zeng, H. Xu, H. Ma, Z. Zhang, J. Peng, S. Duan, Z. Gao, Microglia modulate general anesthesia through $P2Y_{12}$ receptor. *Curr. Biol.* **33**, 2187–2200.e6 (2023).
9. Y. He, T. Liu, Q. He, W. Ke, X. Li, J. Du, S. Deng, Z. Shu, J. Wu, B. Yang, Y. Wang, Y. Mao, Y. Rao, Y. Shu, B. Peng, Microglia facilitate and stabilize the response to general anesthesia via modulating the neuronal network in a brain region-specific manner. *eLife* **12**, RP92252 (2023).
10. J. Peng, Y. Liu, A. D. Umpierre, M. Xie, D. S. Tian, J. R. Richardson, L. J. Wu, Microglial P2Y12 receptor regulates ventral hippocampal CA1 neuronal excitability and innate fear in mice. *Mol. Brain* **12**, 71 (2019).
11. R. L. Lowery, M. S. Mendes, B. T. Sanders, A. J. Murphy, B. S. Whitelaw, C. E. Lamantia, A. K. Majewska, Loss of P2Y12 has behavioral effects in the adult mouse. *Int. J. Mol. Sci.* **22**, 1868 (2021).
12. U. B. Eyo, J. Peng, P. Swiatkowski, A. Mukherjee, A. Bispo, L. J. Wu, Neuronal hyperactivity recruits microglial processes via neuronal NMDA receptors and microglial P2Y12 receptors after status epilepticus. *J. Neurosci.* **34**, 10528–10540 (2014).
13. M. Merlini, V. A. Rafalski, K. Ma, K. Y. Kim, E. A. Bushong, P. E. Rios Coronado, Z. Yan, A. S. Mendiola, E. G. Sozmen, J. K. Ryu, M. G. Haberl, M. Madany, D. N. Sampson, M. A. Petersen, S. Bardehle, R. Tognatta, T. Dean Jr., R. M. Acevedo, B. Cabriga, R. Thomas, S. R. Coughlin, M. H. Ellisman, J. J. Palop, K. Akassoglou, Microglial G(i)-dependent dynamics regulate brain network hyperexcitability. *Nat. Neurosci.* **24**, 19–23 (2021).
14. B. L. Roth, DREADDs for neuroscientists. *Neuron* **89**, 683–694 (2016).
15. S. Zhao, J. Zheng, L. Wang, A. D. Umpierre, S. Parusel, M. Xie, A. Dheer, K. Ayasoufi, A. J. Johnson, J. R. Richardson, L. J. Wu, Chemogenetic manipulation of CX3CR1(+) cells transiently induces hypolocomotion independent of microglia. *Mol. Psychiatry* **28**, 2857–2871 (2023).
16. S. Parusel, M. H. Yi, C. L. Hunt, L. J. Wu, Chemogenetic and optogenetic manipulations of microglia in chronic pain. *Neurosci. Bull.* **39**, 368–378 (2023).
17. A. Dheer, D. B. Bosco, J. Zheng, L. Wang, S. Zhao, K. Haruwaka, M. H. Yi, A. Barath, D. S. Tian, L. J. Wu, Chemogenetic approaches reveal dual functions of microglia in seizures. *Brain Behav. Immun.* **115**, 406–418 (2024).
18. F. Saika, S. Matsuzaki, D. Kobayashi, Y. Ideguchi, T. Y. Nakamura, S. Kishioka, N. Kiguchi, Chemogenetic regulation of CX3CR1-expressing microglia using Gi-DREADD exerts sex-dependent anti-allodynic effects in mouse models of neuropathic pain. *Front. Pharmacol.* **11**, 925 (2020).
19. M. H. Yi, Y. U. Liu, K. Liu, T. Chen, D. B. Bosco, J. Zheng, M. Xie, L. Zhou, W. Qu, L. J. Wu, Chemogenetic manipulation of microglia inhibits neuroinflammation and neuropathic pain in mice. *Brain Behav. Immun.* **92**, 78–89 (2021).
20. Y. Nagai, N. Miyakawa, H. Takuwa, Y. Hori, K. Oyama, B. Ji, M. Takahashi, X. P. Huang, S. T. Slocum, J. F. DiBerto, Y. Xiong, T. Urushihata, T. Hirabayashi, A. Fujimoto, K. Mimura, J. G. English, J. Liu, K. I. Inoue, K. Kumata, C. Seki, M. Ono, M. Shimojo, M. R. Zhang, Y. Tomita, J. Nakahara, T. Suhara, M. Takada, M. Higuchi, J. Jin, B. L. Roth, T. Minamimoto,

Deschloroclozapine, a potent and selective chemogenetic actuator enables rapid neuronal and behavioral modulations in mice and monkeys. *Nat. Neurosci.* **23**, 1157–1167 (2020).
21. H. Wake, A. J. Moorhouse, S. Jinno, S. Kohsaka, J. Nabekura, Resting microglia directly monitor the functional state of synapses in vivo and determine the fate of ischemic terminals. *J. Neurosci.* **29**, 3974–3980 (2009).
22. Y. U. Liu, Y. Ying, Y. Li, U. B. Eyo, T. Chen, J. Zheng, A. D. Umpierre, J. Zhu, D. B. Bosco, H. Dong, L. J. Wu, Neuronal network activity controls microglial process surveillance in awake mice via norepinephrine signaling. *Nat. Neurosci.* **22**, 1771–1781 (2019).
23. R. D. Stowell, G. O. Sipe, R. P. Dawes, H. N. Batchelor, K. A. Lordy, B. S. Whitelaw, M. B. Stoessel, J. M. Bidlack, E. Brown, M. Sur, A. K. Majewska, Noradrenergic signaling in the wakeful state inhibits microglial surveillance and synaptic plasticity in the mouse visual cortex. *Nat. Neurosci.* **22**, 1782–1792 (2019).
24. I. Arganda-Carreras, V. Kaynig, C. Rueden, K. W. Eliceiri, J. Schindelin, A. Cardona, H. Sebastian Seung, Trainable Weka Segmentation: A machine learning tool for microscopy pixel classification. *Bioinformatics* **33**, 2424–2426 (2017).
25. C. Cserep, B. Posfai, A. Denes, Shaping neuronal fate: Functional heterogeneity of direct microglia-neuron interactions. *Neuron* **109**, 222–240 (2021).
26. C. Cserep, B. Posfai, N. Lenart, R. Fekete, Z. I. Laszlo, Z. Lele, B. Orsolits, G. Molnar, S. Heindl, A. D. Schwarcz, K. Ujvari, Z. Kornyei, K. Toth, E. Szabadits, B. Sperlagh, M. Baranyi, L. Csiba, T. Hortobagyi, Z. Magloczky, B. Martinecz, G. Szabo, F. Erdelyi, R. Szipocs, M. M. Tamkun, B. Gesierich, M. Duering, I. Katona, A. Liesz, G. Tamas, A. Denes, Microglia monitor and protect neuronal function through specialized somatic purinergic junctions. *Science* **367**, 528–537 (2020).
27. E. Smedler, S. Malmersjö, P. Uhlén, Network analysis of time-lapse microscopy recordings. *Front. Neural Circuits* **8**, 111 (2014).
28. C. C. Hsiao, R. Sankowski, M. Prinz, J. Smolders, I. Huitinga, J. Hamann, GPCRomics of homeostatic and disease-associated human microglia. *Front. Immunol.* **12**, 674189 (2021).
29. S. E. Haynes, G. Hollopeter, G. Yang, D. Kurpius, M. E. Dailey, W. B. Gan, D. Julius, The P2Y12 receptor regulates microglial activation by extracellular nucleotides. *Nat. Neurosci.* **9**, 1512–1519 (2006).
30. T. Chen, V. A. Lennon, Y. U. Liu, D. B. Bosco, Y. Li, M.-H. Yi, J. Zhu, S. Wei, L.-J. Wu, Astrocyte-microglia interaction drives evolving neuromyelitis optica lesion. *J. Clin. Invest.* **130**, 4025–4038 (2020).
31. G. Milior, C. Lecours, L. Samson, K. Bisht, S. Poggini, F. Pagani, C. Deflorio, C. Lauro, S. Alboni, C. Limatola, I. Branchi, M. E. Tremblay, L. Maggi, Fractalkine receptor deficiency impairs microglial and neuronal responsiveness to chronic stress. *Brain Behav. Immun.* **55**, 114–125 (2016).
32. A. D. Umpierre, L. L. Bystrom, Y. Ying, Y. U. Liu, G. Worrell, L. J. Wu, Microglial calcium signaling is attuned to neuronal activity in awake mice. *eLife* **9**, e56502 (2020).
33. C. Ma, B. Li, D. Silverman, X. Ding, A. Li, C. Xiao, G. Huang, K. Worden, S. Muroy, W. Chen, Z. Xu, C. F. Tso, Y. Huang, Y. Zhang, Q. Luo, K. Saijo, Y. Dan, Microglia regulate sleep through calcium-dependent modulation of norepinephrine transmission. *Nat. Neurosci.* **27**, 249–258 (2024).
34. A. D. Umpierre, B. Li, K. Ayasoufi, W. L. Simon, S. Zhao, M. Xie, G. Thyen, B. Hur, J. Zheng, Y. Liang, D. B. Bosco, M. A. Maynes, Z. Wu, X. Yu, J. Sung, A. J. Johnson, Y. Li, L.-J. Wu, Microglial $P2Y_6$ calcium signaling promotes phagocytosis and shapes neuroimmune responses in epileptogenesis. *Neuron* **112**, 1959–1977.e10 (2024).
35. V. Konieczny, S. C. Tovey, S. Mataragka, D. L. Prole, C. W. Taylor, Cyclic AMP recruits a discrete intracellular Ca(2+) store by unmasking hypersensitive IP(3) receptors. *Cell Rep.* **18**, 711–722 (2017).
36. S. C. Tovey, S. G. Dedos, E. J. Taylor, J. E. Church, C. W. Taylor, Selective coupling of type 6 adenylyl cyclase with type 2 IP_3 receptors mediates direct sensitization of IP_3 receptors by cAMP. *J. Cell Biol.* **183**, 297–311 (2008).
37. L. P. Bernier, C. J. Bohlen, E. M. York, H. B. Choi, A. Kamyabi, L. Dissing-Olesen, J. K. Hefendehl, H. Y. Collins, B. Stevens, B. A. Barres, B. A. MacVicar, Nanoscale surveillance of the brain by microglia via cAMP-regulated filopodia. *Cell Rep.* **27**, 2895–2908.e4 (2019).
38. S. Roychowdhury, M. M. Rasenick, Submembraneous microtubule cytoskeleton: Regulation of microtubule assembly by heterotrimeric Gproteins. *FEBS J.* **275**, 4654–4663 (2008).
39. S. Roychowdhury, D. Panda, L. Wilson, M. M. Rasenick, G protein alpha subunits activate tubulin GTPase and modulate microtubule polymerization dynamics. *J. Biol. Chem.* **274**, 13485–13490 (1999).
40. I. Schubert, R. Ahlbrand, A. Winter, L. Vollmer, I. Lewkowich, R. Sah, Enhanced fear and altered neuronal activation in forebrain limbic regions of CX3CR1-deficient mice. *Brain Behav. Immun.* **68**, 34–43 (2018).
41. R. Akiyoshi, H. Wake, D. Kato, H. Horiuchi, R. Ono, A. Ikegami, K. Haruwaka, T. Omori, Y. Tachibana, A. J. Moorhouse, J. Nabekura, Microglia enhance synapse activity to promote local network synchronization. *eNeuro* **5**, ENEURO.0088-18.2018 (2018).
42. C. N. Parkhurst, G. Yang, I. Ninan, J. N. Savas, J. R. Yates III, J. J. Lafaille, B. L. Hempstead, D. R. Littman, W. B. Gan, Microglia promote learning-dependent synapse formation through brain-derived neurotrophic factor. *Cell* **155**, 1596–1609 (2013).
43. P. T. Nguyen, L. C. Dorman, S. Pan, I. D. Vainchtein, R. T. Han, H. Nakao-Inoue, S. E. Taloma, J. J. Barron, A. B. Molofsky, M. A. Kheirbek, A. V. Molofsky, Microglial remodeling of the extracellular matrix promotes synapse plasticity. *Cell* **182**, 388–403.e15 (2020).
44. H. Liu, X. Wang, L. Chen, L. Chen, S. E. Tsirka, S. Ge, Q. Xiong, Microglia modulate stable wakefulness via the thalamic reticular nucleus in mice. *Nat. Commun.* **12**, 4646 (2021).
45. M. J. Pinto, L. Cottin, F. Dingli, V. Laigle, L. F. Ribeiro, A. Triller, F. Henderson, D. Loew, V. Fabre, A. Bessis, Microglial TNFα orchestrates protein phosphorylation in the cortex during the sleep period and controls homeostatic sleep. *EMBO J.* **42**, e111485 (2023).
46. I. Hristovska, M. Robert, K. Combet, J. Honnorat, J. C. Comte, O. Pascual, Sleep decreases neuronal activity control of microglial dynamics in mice. *Nat. Commun.* **13**, 6273 (2022).
47. S. K. Chen, P. Tvrdik, E. Peden, S. Cho, S. Wu, G. Spangrude, M. R. Capecchi, Hematopoietic origin of pathological grooming in Hoxb8 mutant mice. *Cell* **141**, 775–785 (2010).
48. A. S. Warden, S. A. Wolfe, S. Khom, F. P. Varodayan, R. R. Patel, M. Q. Steinman, M. Bajo, S. E. Montgomery, R. Vlkolinsky, T. Nadav, I. Polis, A. J. Roberts, R. D. Mayfield, R. A. Harris, M. Roberto, Microglia control escalation of drinking in alcohol-dependent mice: Genomic and synaptic drivers. *Biol. Psychiatry* **88**, 910–921 (2020).
49. M. Zhuo, G. Wu, L. J. Wu, Neuronal and microglial mechanisms of neuropathic pain. *Mol. Brain* **4**, 31 (2011).
50. U. B. Eyo, M. Murugan, L. J. Wu, Microglia-neuron communication in epilepsy. *Glia* **65**, 5–18 (2017).
51. U. Eyo, A. V. Molofsky, Defining microglial-synapse interactions. *Science* **381**, 1155–1156 (2023).
52. A. Venturino, R. Schulz, H. De Jesus-Cortes, M. E. Maes, B. Nagy, F. Reilly-Andujar, G. Colombo, R. J. A. Cubero, F. E. Schoot Uiterkamp, M. F. Bear, S. Siegert, Microglia enable mature perineuronal nets disassembly upon anesthetic ketamine exposure or 60-Hz light entrainment in the healthy brain. *Cell Rep.* **36**, 109313 (2021).
53. P. Jiang, F. Xing, B. Guo, J. Yang, Z. Li, W. Wei, F. Hu, I. Lee, X. Zhang, L. Pan, J. Xu, Nucleotide transmitters ATP and ADP mediate intercellular calcium wave communication via P2Y12/13 receptors among BV-2 microglia. *PLOS ONE* **12**, e0183114 (2017).
54. K. Farber, H. Kettenmann, Functional role of calcium signals for microglial function. *Glia* **54**, 656–665 (2006).
55. M. H. Yi, Y. U. Liu, A. D. Umpierre, T. Chen, Y. Ying, J. Zheng, A. Dheer, D. B. Bosco, H. Dong, L. J. Wu, Optogenetic activation of spinal microglia triggers chronic pain in mice. *PLOS Biol.* **19**, e3001154 (2021).
56. S. Koizumi, Y. Shigemoto-Mogami, K. Nasu-Tada, Y. Shinozaki, K. Ohsawa, M. Tsuda, B. V. Joshi, K. A. Jacobson, S. Kohsaka, K. Inoue, UDP acting at P2Y6 receptors is a mediator of microglial phagocytosis. *Nature* **446**, 1091–1095 (2007).
57. A. M. Klawonn, M. Fritz, S. Castany, M. Pignatelli, C. Canal, F. Simila, H. A. Tejeda, J. Levinsson, M. Jaarola, J. Jakobsson, J. Hidalgo, M. Heilig, A. Bonci, D. Engblom, Microglial activation elicits a negative affective state through prostaglandin-mediated modulation of striatal neurons. *Immunity* **54**, 225–234.e6 (2021).
58. J. Bossuyt, Y. Van Den Herrewegen, L. Nestor, A. Buckinx, D. De Bundel, I. Smolders, Chemogenetic modulation of astrocytes and microglia: State-of-the-art and implications in neuroscience. *Glia* **71**, 2071–2095 (2023).
59. P. M. Grace, K. A. Strand, E. L. Galer, D. J. Urban, X. Wang, M. V. Baratta, T. J. Fabisiak, N. D. Anderson, K. Cheng, L. I. Greene, D. Berkelhammer, Y. Zhang, A. L. Ellis, H. H. Yin, S. Campeau, K. C. Rice, B. L. Roth, S. F. Maier, L. R. Watkins, Morphine paradoxically prolongs neuropathic pain in rats by amplifying spinal NLRP3 inflammasome activation. *Proc. Natl. Acad. Sci. U.S.A.* **113**, E3441–E3450 (2016).
60. P. M. Grace, X. Wang, K. A. Strand, M. V. Baratta, Y. Zhang, E. L. Galer, H. Yin, S. F. Maier, L. R. Watkins, DREADDed microglia in pain: Implications for spinal inflammatory signaling in male rats. *Exp. Neurol.* **304**, 125–131 (2018).
61. Tabula Muris Consortium, Overall coordination, Logistical coordination, Organ collection and processing, Library preparation and sequencing, Computational data analysis, Cell type annotation, Writing group, Supplemental text writing group, Principal investigators, Single-cell transcriptomics of 20 mouse organs creates a *Tabula Muris*. *Nature* **562**, 367–372 (2018).
62. Y. Hao, S. Hao, E. Andersen-Nissen, W. M. Mauck III, S. Zheng, A. Butler, M. J. Lee, A. J. Wilk, C. Darby, M. Zager, P. Hoffman, M. Stoeckius, E. Papalexi, E. P. Mimitou, J. Jain, A. Srivastava, T. Stuart, L. M. Fleming, B. Yeung, A. J. Rogers, J. M. McElrath, C. A. Blish, R. Gottardo, P. Smibert, R. Satija, Integrated analysis of multimodal single-cell data. *Cell* **184**, 3573–3587.e29 (2021).

Acknowledgments: We thank members of the Wu lab for insightful discussions. **Funding:** This work was supported by the following grants: National Institutes of Health grants R35NS132326 (L.-J.W.) and R00NS126417 (A.D.U.) **Author contributions:** Writing–original draft: S.Z., L.W., and L.-J.W.; conceptualization: S.Z. and L.-J.W.; investigation: S.Z., L.W., F.Q., Y.L., and J.Z.; writing–review and editing: S.Z., L.-J.W., and A.D.U.; methodology: S.Z. and L.-J.W.; data curation: S.Z. and L.W.; validation: S.Z., L.W., and F.Q.; formal analysis: S.Z., L.W., D.K, and F.Q.; visualization: S.Z., L.W., and L.-J.W.; software: L.W.; resources: L.-J.W.; funding acquisition: L.-J.W. and A.D.U.;

supervision: L.-J.W.; and project administration: L.-J.W. **Competing interests:** The authors declare that they have no competing interests. **Data and materials availability:** All data needed to evaluate the conclusions in the paper are present in the paper and/or the Supplementary Materials.

Submitted 22 February 2024
Accepted 29 January 2025
Published 28 February 2025
10.1126/sciadv.ado7829